

RESEARCH

Open Access



MPTP mediated Ox-mtDNA release inducing macrophage pyroptosis and exacerbating MCD-induced MASH via promoting the ITPR3/ Ca^{2+} /NLRP3 pathway

Qi Zhang¹, Li Chen², Jun-Yan Liu¹, Tao Liu³, Rui Wang¹, Xin-Yi Wu^{1*} and Sheng-Wei Li^{1*}

Abstract

Background Metabolic Dysfunction-Associated Steatohepatitis (MASH) is a severe and progressive form of Metabolic Dysfunction-Associated Steatotic Liver Disease (MASLD), with approximately 25% of adults worldwide suffering from MASLD, of which 20%-30% progress to MASH, and the global incidence continues to rise. Oxidized mitochondrial DNA (Ox-mtDNA) release is a key contributor to MASH. However, its underlying mechanism remains unclear. Clarifying this process may provide a theoretical foundation for MASH treatment.

Methods In this study, we separately established MASH models using methionine- and choline deficient diet (MCD) fed mice *in vivo* and free fatty acid (FFA)-stimulated THP-1 derived macrophages *in vitro*. Cyclosporin A (CsA: mitochondrial permeability transition pore, mPTP, channel inhibitor) was used to inhibit the release of Ox-mtDNA. 8-OH-dG detection and fluorescent probe were used to evaluate Ox-mtDNA release. Liver lipid deposition was analyzed by Triglyceride (TG) and Oil Red O, and tissue damage were analyzed by aspartate transaminase and alanine aminotransferase (ALT, AST) and H&E staining. Pyroptosis markers, such as cleaved-Caspase1, GSDMD-N, and inflammatory cytokines, such as interleukin – 1 β , interleukin 18 (IL-1 β , IL-18), were detected by WB, ELISA and transmission electron microscopy (TEM) experiments, and the key pyroptosis pathways activated by Ox-mtDNA were screened by RNA-seq. Finally, ITPR3 was silenced by siRNA *in vitro* and by Adeno-associated virus (AAV) *in vivo* respectively, which confirmed the role of ITPR3/ Ca^{2+} /NLRP3 axis in Ox-mtDNA regulating macrophage pyroptosis mediated MASH.

Results The cytosolic Ox-mtDNA level was significantly increased during MASH. Inhibition of Ox-mtDNA release alleviated macrophage pyroptosis to improve the pathological phenotype of MASH. RNA-seq analysis showed that cytosolic Ox-mtDNA triggered an inflammatory response by activating the NOD-like receptor pathway, in which FFA induced upregulation of inositol 1,4,5-Trisphosphate Receptor Type 3 (ITPR3, IP3R) expression, and Inhibition of Ox-mtDNA release could relieve this effect. ITPR3 silencing significantly reduced Ca^{2+} release, which in turn inhibited

*Correspondence:

Xin-Yi Wu
1121790213@qq.com
Sheng-Wei Li
lishengwei@hospital.cqmu.edu.cn

Full list of author information is available at the end of the article



© The Author(s) 2025. **Open Access** This article is licensed under a Creative Commons Attribution-NonCommercial-NoDerivatives 4.0 International License, which permits any non-commercial use, sharing, distribution and reproduction in any medium or format, as long as you give appropriate credit to the original author(s) and the source, provide a link to the Creative Commons licence, and indicate if you modified the licensed material. You do not have permission under this licence to share adapted material derived from this article or parts of it. The images or other third party material in this article are included in the article's Creative Commons licence, unless indicated otherwise in a credit line to the material. If material is not included in the article's Creative Commons licence and your intended use is not permitted by statutory regulation or exceeds the permitted use, you will need to obtain permission directly from the copyright holder. To view a copy of this licence, visit <http://creativecommons.org/licenses/by-nc-nd/4.0/>.

nucleotide-binding domain and leucine-rich repeat protein-3 (NLRP3) inflammasome activation and macrophage pyroptosis. Cytosolic Ox-mtDNA promotes Ca^{2+} release by upregulating ITPR3, activates NLRP3-dependent macrophage pyroptosis, and ultimately exacerbates liver injury and MASH progression.

Conclusions This study demonstrates that Ox-mtDNA drives MASH progression by promoting macrophage pyroptosis via the ITPR3/ Ca^{2+} /NLRP3 axis, providing a novel therapeutic strategy for targeted intervention.

Keywords MASH, Ox-mtDNA, Pyroptosis, ITPR3, Ca^{2+} , NLRP3

Introduction

Metabolic Dysfunction-Associated Steatohepatitis (MASH), the progressive form of Metabolic Dysfunction-Associated Steatotic Liver Disease (MASLD), pose a significant global health concern, affecting approximately 20%-25% of the population [1]. This condition can lead to liver fibrosis, cirrhosis, and even hepatocellular carcinoma (HCC) [2, 3]. MASH is also the main indication for liver transplantation because it is associated with the risk of progression to end-stage liver disease [4]. Therefore, there is an urgent need to elucidate the pathogenesis of MASH in order to develop effective treatments.

The liver innate immune system plays a key role in the pathogenesis of MASH, involving coordinated interactions between immune cells such as liver macrophages, Natural Killer Cells (NK cells), Type 1 Congenital Lymphoid Cells (ILC1), and neutrophils [5, 6]. NK cells/ILC1 promote M1 macrophage polarization through Interferon-gamma (IFN- γ) and Tumor Necrosis Factor-alpha (TNF- α), while exerting anti-fibrotic effects [7–9]. Neutrophils cause early hepatocyte damage through the formation of elastases and neutrophil extracellular traps (NETs) [10]. Notably, hepatic macrophages induce inflammation by sensing pathogen-associated molecular patterns/damage-associated molecular patterns (PAMPs/DAMPs) and metabolites (e.g., FFA) and secrete chemokines to recruit and activate other immune cells [11]. It is the main immune cell that coordinates inflammation and fibrosis [7, 12]. Therefore, it is of great significance to explore the mechanism of immune-inflammatory mediation mediated by liver macrophages in MASH.

The pathogenesis of MASH involves chronic inflammation and progressive hepatocellular injury with fibrosis [13, 14], with macrophage pyroptosis being a key pathologic event [15]. Pyroptosis is mediated by the nucleotide-binding domain and leucine-rich repeat protein-3 (NLRP3) inflammasome-Gasdermin D (GSDMD) signaling axis, triggering programmed cell death [16, 17]. NLRP3 inflammasome activates Caspase1, cleaves GSDMD, releases GSDMD-N, and its oligomerization forms membrane pores (10–20 nm), resulting in osmotic imbalance, pyroptosis, and the release of inflammatory factors such as IL-1 β /IL-18 [18, 19]. However, in MASH, the factors and mechanisms that induce pyroptosis in macrophages have not been fully elucidated [20, 21].

Oxidized mitochondrial DNA (Ox-mtDNA), a characteristic damage molecule resulting by cytosolic reactive oxygen species (ROS) attack, inducing inflammatory cascades through activating the NLRP3 inflammasome [22]. Recent studies demonstrate Ox-mtDNA's critical role in various pathologies, including metabolic diseases (e.g., MASH) [23], autoimmune disorders, and neurodegenerative diseases [24, 25]. Notably, Ox-mtDNA has been shown to regulate macrophage pyroptosis in both cellular and mouse models [26]. However, its exact molecular mechanisms and therapeutic potential in MASH require further investigation.

Inositol 1,4,5-triphosphate receptor type 3 (ITPR3, IP3R) is a key channel protein for endoplasmic reticulum (ER)-mediated calcium ions (Ca^{2+}) release [27], and recent studies have shown that ITPR3-mediated Ca^{2+} release promotes LPS-induced cardiomyocyte pyroptosis [28]. However, in MASH, it is unclear whether Ox-mtDNA mediates macrophage pyroptosis via the ITPR3/ Ca^{2+} /NLRP3 axis or not.

In this study, we used MCD to build a MASH model [29–31], and the results showed that Ox-mtDNA was significantly upregulated in free fatty acid (FFA)-treated THP-1 derived macrophages and MCD animal model, and pyroptosis occurs in macrophages. We found that ITPR3 is a key reactive protein downstream of Ox-mtDNA by RNA-seq. Furthermore, ITPR3 activated NLRP3 inflammasome by promoting the release of Ca^{2+} the ER. Pharmacological inhibition of Ox-mtDNA release was found to significantly attenuate ITPR3/ Ca^{2+} /NLRP3 signaling axis activity, accompanied by significant reductions in macrophage pyroptosis. These findings provide evidence that the ITPR3/ Ca^{2+} /NLRP3 axis is a key mechanism of Ox-mtDNA influencing macrophage pyroptosis and aggravating MCD animal model, which is expected to provide some basic theory for clinical research on MASH.

Materials and methods

Animal experiment

MASH animal model

Male wild-type (WT) C57BL/6 mice (6–8 weeks, $n=6$ /group) were purchased by the Experimental Animal Center of Chongqing Medical University (IACUC-CQMU-2025-0304), initially weighing 19.7 ± 0.7 g, were

used in the present study. The MASH animal model was established according to the previous report (use MCD: Research Diets, A02082002BR). After adapting for one week, the mice were maintained in an animal room with controlled conditions: light/dark cycle of 12 h/12 h, $22 \pm 2^\circ\text{C}$, and humidity of 55%–65%. Humane care guided by the guidelines of the National Institutes of Health was provided to all animals. All mice were raised under specific pathogen-free conditions, following the procedures approved by the Animal Use and Ethics Committee of the 2nd Affiliated Hospital of Chongqing Medical University.

Animals were randomly divided and there were 6 mice in each group: (1) SHAM group: Mice were raised with normal food. (2) MCD group: Mice were raised on MCD feed. (3) MCD + CsA group: the cyclosporin A (CsA), a specific inhibitor of the mPTP (10 mg/kg/day), blocked the release of Ox-mtDNA by gavage for 7 weeks, and began to establish the MCD model after 3 weeks. (4) MCD + DMSO group: 1% DMSO working solution (1% DMSO, 40% PEG300, 5% Tween 80, and 54% ddH₂O) was prepared and given gavage in equal parts with CsA. (5) MCD ITPR3-AAV group: AAV-F4/80-ITPR3-EGFP-specific silenced liver macrophage ITPR3, titer was 1.5×10^{11} TU/mL (interference sequence: CAGCUGGA AGAUCAACUUUU), mice were adaptively fed for 1 week, injected through tail vein. The MCD model was constructed after 4 weeks. (6) MCD + NC group: adenovirus containing only blank vector (NC) was injected into the tail vein with a titer of 1.5×10^{11} TU/mL, and the MCD animal model was constructed after 4 weeks.

Isolation and cultivation of liver macrophages

Primary liver macrophages were isolated from normal liver tissue using a three-step enzymatic-mechanical dissociation protocol adapted from Li et al. [32], involving: (1) collagenase IV (Sigma-Aldrich) digestion, (2) density gradient centrifugation, and (3) selective adherence purification. Isolated cells were maintained in complete DMEM medium (Gibco) supplemented with 10% fetal bovine serum (Gibco), 100U/mL penicillin G, and 100U/mL streptomycin (both from Beyotime), under standard culture conditions (37°C , 5% CO₂ humidified atmosphere). Finally, the separation effect was verified by flow cytometry (Fig. S1. A).

H&E staining

H&E staining was applied for detecting pathological changes in the liver. Fresh liver tissue was fixed with 4% paraformaldehyde, embedded in paraffin, and sliced (the thickness was 4 μm). After dewaxing and hydrating, the slices were stained with hematoxylin (Sigma, Shanghai, China) at room temperature (RT), and then rinsed. After differentiating with 5% acetic acid for 1 min, the

slices were rinsed and then stained with eosin (Sigma) for 1 min.

NAS scoring

The most commonly used NAS score is a semi-quantitative scoring system, in which hepatocyte steatosis is 0–3 points, balloon-like degeneration is 0–2 points, and inflammation is 0–3 points, with a total score of 8 points. The NAS score was obtained by adding the above three scores: hepatocyte steatosis, hepatocyte ballooning, and intralobular inflammation. A NAS score of ≥ 5 is diagnostic of MASH; A NAS score of 3 to 4 suspects nonalcoholic steatohepatitis; A NAS score of < 3 does not diagnose nonalcoholic steatohepatitis. All scoring is blinded.

Oil red O staining

To stain triglycerides (TG), frozen liver tissue sections (5 μM) or THP-1 derived macrophages were washed twice with PBS and fixed in 4% paraformaldehyde for 10 min at RT. After two additional PBS washes, samples were stained using an Oil Red O Kit (Beyotime, C0158S) following the manufacturer's instructions. Excess stain was removed, and samples were rinsed three times with distilled water before microscopic examination. The Olympus inverted fluorescence microscope IX73 was used for capture at 20x. Finally, imageJ (win-64) was used to quantify the entire image.

Immunohistochemical staining (IHC)

The paraffin-embedded sections were first heated in a 60 °C oven, followed by deparaffinization through immersion in xylene and a graded ethanol series. For antigen retrieval, the slides were microwaved in Tris-EDTA buffer (Beyotime) at medium-high power for 8 min and then at medium-low power for 20 min, before cooling to RT. Endogenous peroxidase activity was blocked by incubating the sections with 3% hydrogen peroxide for 10 min at RT. After PBS washing, the sections were probed overnight at 4 °C with primary antibodies against Caspase1 (1:500, Huabio) and GSDMD (1:400, Abcam). Unbound antibodies were removed by PBS rinsing, and the sections were then treated with an IHC Kit reagents (including enhancer and IgG polymer, AiFang Biological) at RT. Immunoreactivity was visualized using 3,3'-diaminobenzidine (DAB), followed by haematoxylin counterstaining. Finally, the slides were dehydrated in an ascending ethanol series and xylene, mounted with neutral gum, and examined under a light microscope. Finally, imageJ (win-64) was used to quantify the entire image.

Biochemical analysis

Serum samples were used for biochemical analysis. Alanine aminotransferase (ALT) and aspartate

aminotransferase (AST) were measured using the ALT/AST Kit (Solarbio, BC1555/BC1565). Please refer to the instructions for specific steps.

Triglyceride content detection

The triglyceride (TG) test Kit (Solarbio, BC0625) was used to analyze the liver TG level according to the manufacturer's instructions. Weigh about 0.1g of liver tissue, add 1mL of n-heptane and isopropanol mixture for ice bath homogenization, 8000g, centrifuge at 4 degrees for 10 min. Take the supernatant and read the absorbance at 420 nm with a microplate reader (Thermo Fisher Scientific).

Cell culture and treatment

THP-1 derived macrophages were cultured in RPMI-1640 (Gibco) supplemented with 10% fetal bovine serum (Pricella, 164210-50) and antibiotics (Hyclone, HYC-SV 30010) in a cell culture incubator with 5% CO₂ at 37 °C until the logarithmic growth phase. Using Phorbol 12-myristate 13-acetate (PMA: 100ng/mL) to induce THP-1 derived macrophages adherence (24 h) and validate their differentiation in macrophages (Fig. S1. B). THP-1 derived macrophages were cultured with 0.5mM concentration of FFA for 24 h to establish an in vitro model. In addition, the cells were treated in advance using 1μM CsA (MCE, HY-B0579) for 24 h to inhibit the opening of mPTP channels. Use DMSO as a negative control. To knock down ITPR3 in vitro, siITPR3 was pre-transfected into THP-1 derived macrophages using Lipofectamine 2000 (Invitrogen, USA). In some experiments, cells were incubated with ionomycin (4μM) (MCE: HY-13434) for 8 h to increase intracellular Ca²⁺ levels. Diphenyleneiodonium chloride (DPI: 10μM) is a ROS scavenger and will be used in some experiments (MCE: HY-100965).

Configuration of FFA

Palmitic acid-BSA conjugate

Solution A: 0.2g NaOH in 50mL ddH₂O; Solution B: 0.9188g palmitic acid (sigma, P0500) solution was added to 50mL of solution A and heated at 80 °C until clear; Solution C: 1g BSA (Beyotime, ST023-50g) in 10mL ddH₂O. Next at 55 °C, slowly add 50μL Solution B to 950μL Solution C. Finally, 0.22μM filter, then store at 4 °C in a dark place.

Oleic acid-BSA conjugate

Solution A: 2.0094g sodium oleate (sigma, O7501-250MG) in 50mL ddH₂O; Solution B: 1g BSA in 10mL ddH₂O. Next at 55 °C, slowly add 50μL Solution A to 950μL Solution B. Finally, 0.22μM filter, then store at 4 °C in a dark place.

ELISA

IL-1β and IL-18 levels in mouse serum or THP-1 derived macrophages supernatant were quantified using commercial ELISA Kits (Beyotime, PI553 and PI301) according to the manufacturer's instructions. Briefly, 50μL of each sample was added to the wells, followed by 100μL of HRP-conjugated detection antibody. The plate was sealed and incubated at 37 °C for 60 min. After aspiration, wells were washed five times with wash buffer. Next, 50μL each of substrate A and B was added, followed by a 15 min incubation at 37 °C. The reaction was stopped with 50μL stop solution, and absorbance was measured at 450 nm within 15 min. Sample concentrations were determined from the standard curve.

Western blot (WB)

Protein samples were extracted from cells or tissues using RIPA lysis buffer (Beyotime) supplemented with 1× protease phosphatase inhibitor cocktail (Beyotime). Following lysis, samples were centrifuged at 12,000×g for 15 min at 4 °C, and the supernatant was collected for protein quantification using a BCA Protein Assay Kit (Beyotime). Equal amounts of protein were mixed with 5× SDS-PAGE loading buffer, denatured at 100 °C for 10 min, and separated by SDS-PAGE.

After electrophoresis, proteins were transferred to PVDF membranes, which were then blocked with 5% BSA for 1 h at RT. The membranes were probed with primary antibodies overnight at 4 °C, followed by incubation with HRP-conjugated secondary antibodies (1:8000, BOSTER) for 1 h at RT. Protein bands were visualized using a Bio-Rad Universal Hood III imaging system and quantified using ImageJ Lab software (version 3.0). All antibodies used in this study are listed in Table 1.

RT-qPCR

High-quality total RNA was rapidly extracted using the RNA-Quick Purification Kit (ESscience, ES-RN001) and cDNA was obtained using reverse transcription. The reverse transcription conditions were: 25 °C for 5 min; 55 °C for 15 min; 85 °C for 2 min. qRT-PCR analysis was performed using SYBR Green qPCR Master Mix (No ROX, HY-K0523, MCE). β-Actin was used as internal controls. The 2^{-ΔΔCt} method was used to calculate the relative expression. The primers used for RT-PCR analysis are as follows:

ITPR3(human) forward: ACGGACGAGGAGGGCTTT CTG.
ITPR3(human) reverse: AACCCCGCACATCTTGTCA GC.

ITPR3(mouse) forward: CCCACCAATGCTGACATCC T.
ITPR3(mouse) reverse: ACCTCTTCCTCATCCTCCCC.

Mitochondrial isolation protocol

HB Buffer Preparation: Prepare ice-cold HB buffer (250mM sucrose, 10mM HEPES, pH 7.4) with 1× protease phosphatase inhibitor cocktail. Cell Homogenization: Harvest liver macrophages or THP-1 derived macrophages, resuspend in 1mL chilled HB buffer, incubate on ice for 10 min, and homogenized on ice using a 22G needle. Fractionation: Centrifuge homogenate at 1,100×g (10 min, 4 °C), collect supernatant (whole cell extract), and discard pellet (nuclear fraction/debris). Further centrifuge supernatant at 11,000×g (15 min, 4 °C) to separate cytosolic fraction (supernatant) and mitochondrial fraction (pellet). Mitochondrial Purification: Wash mitochondrial pellet with 1mL HB buffer, re-centrifuge (11,000×g, 15 min, 4 °C), and resuspend in 100 – 150µL HB buffer. Quality Control: Measure protein concentration via BCA assay and validate isolation by Western blot using β-Actin (cytosolic marker) and COX IV (mitochondrial marker). This protocol ensures efficient mitochondrial isolation while maintaining integrity for downstream analyses. Finally, the separation effect was verified by WB technology (Fig. S1. C-D).

Measurement of MtDNA

Following DNA extraction from whole cell extracts and cytosolic fractions using the BeyoMag™ Magnetic Bead PCR/DNA Purification Kit (D0041, Beyotime), mitochondrial DNA (mtDNA) levels were quantified by real-time quantitative PCR with SYBR Green qPCR Master Mix (No ROX, HY-K0523, MCE). Mitochondrial-specific primer pairs (sequences listed in Table 2) were used for amplification, with all procedures performed according to the manufacturers' protocols.

Measurement of oxidized MtDNA (Ox-mtDNA)

To quantify oxidized mitochondrial DNA (Ox-mtDNA), we isolated mtDNA from either cytosolic or mitochondrial fractions using the aforementioned protocol, followed by measurement of 8-hydroxy-2'-deoxyguanosine (8-OH-dG) levels using a commercial ELISA Kit (Abcam, ab285254) according to the manufacturer's instructions.

Co-localization of mitochondria and DsDNA

Following the 1/2 small volume infection protocol, THP-1 derived macrophages were transduced with PlvW-CMV-Mito-mCherry-EF1-puro (Red) (Hunan LeapWal Biotech Co., Ltd.) lentiviral particles, and transfection efficiency was assessed by fluorescence microscopy. For mitochondrial DNA visualization, cells were stained with SYBR™ Gold nucleic acid gel (Invitrogen, S11494) stain (1:10,000 dilution in PBS) for 30 min at 37 °C, followed by three PBS washes prior to confocal imaging, as per the manufacturer's specifications. Images were acquired at 600x using an Olympus microscope.

Mitochondrial structure observation

According to the 1/2 small volume infection protocol, THP-1-derived macrophages were transduced by PlvW-CMV-mitoEGFP-EF1-puro (OE) lentiviral particles (Hunan LeapWal Biotech Co., Ltd.). Mitochondrial structure was observed using a fluorescence confocal microscope. Images were acquired at 600x using an Olympus microscope.

Measurement of intracellular Ca²⁺

Following the manufacturer's protocol (Beyotime, S1061S), THP-1 derived macrophages were loaded with 1µM Fluo-4 AM by incubating at 37 °C for 30 min under light-protected conditions. Intracellular Ca²⁺ signals were subsequently quantified by measuring fluorescence intensity using the Olympus inverted fluorescence microscope IX73 was used for capture at 20x.

Measurement of mPTP channel opening

Following the manufacturer's protocol (Beyotime, C2009S), THP-1 derived macrophages were incubated with 1× calcein and 1× CoCl₂ in the dark at 37 °C for 30 min. After three washes with PBS, cellular fluorescence was immediately examined using the Olympus inverted fluorescence microscope IX73 was used for capture at 20x.

Caspase1 activity

Caspase1 enzymatic activity was assessed in both primary liver macrophages and THP-1 derived macrophages using a fluorometric Caspase1 activity assay Kit (Beyotime, C1101), with all procedures performed in strict accordance with the manufacturer's instructions.

LDH release assay

According to the manufacturer's protocol, LDH in mouse serum or THP-1 derived macrophages supernatant was quantitated by the LDH activity assay Kit (Abcam, ab65391) The absorbance was read at 490 nm with a microplate reader (Thermo Fisher Scientific).

Transmission electron microscopy (TEM)

Liver tissues collected from mice were dissected into 1 mm³ fragments and fixed in 3% glutaraldehyde, while macrophages were pelleted by centrifugation (12,000×g, 10 min) and similarly fixed. All samples were processed and analyzed by transmission electron microscopy (TEM) at the Electron Microscopy Center of Chengdu Lilai Biotech Co., Ltd.

Mitochondrial swelling score

0. points: The mitochondrial ultrastructure is normal, the particles are intact, and there are no abnormal manifestations such as swelling.
1. point: Mild swelling of mitochondria, slight decrease in matrix electron density, slight expansion and disorder of the crest, but the overall structure is basically intact.
2. points: mitochondrial swelling is more obvious, matrix electron density is significantly reduced, the crest is obviously expanded and disordered, and some crest is broken.
3. points: Mitochondria are severely swollen, the electron density of the matrix is extremely low, a large number of crests are broken and disappear, and the mitochondrial membrane structure begins to show abnormalities.
4. points: Severe swelling of mitochondria, loss of integrity of mitochondrial membranes, vacuolization, rupture and other phenomena.

Flow cytometry (FC)

Digest primary macrophages at RT, terminate digestion 1:1 using complete medium, collect in flow cytometry tubes, and wash three times with PBS. Staining with 0.5 μ g F4/80 antibody (11-4801-82, invitrogen) for 30 min, followed by 0.25 μ g CD68 antibody (98029-1-RR, protein-tech) for 30 min. When using CD68, the cells were fixed with 4% paraformaldehyde (PFA) and permeabilized with flow cytometry permeabilization buffer (PF00011-C, proteintech).

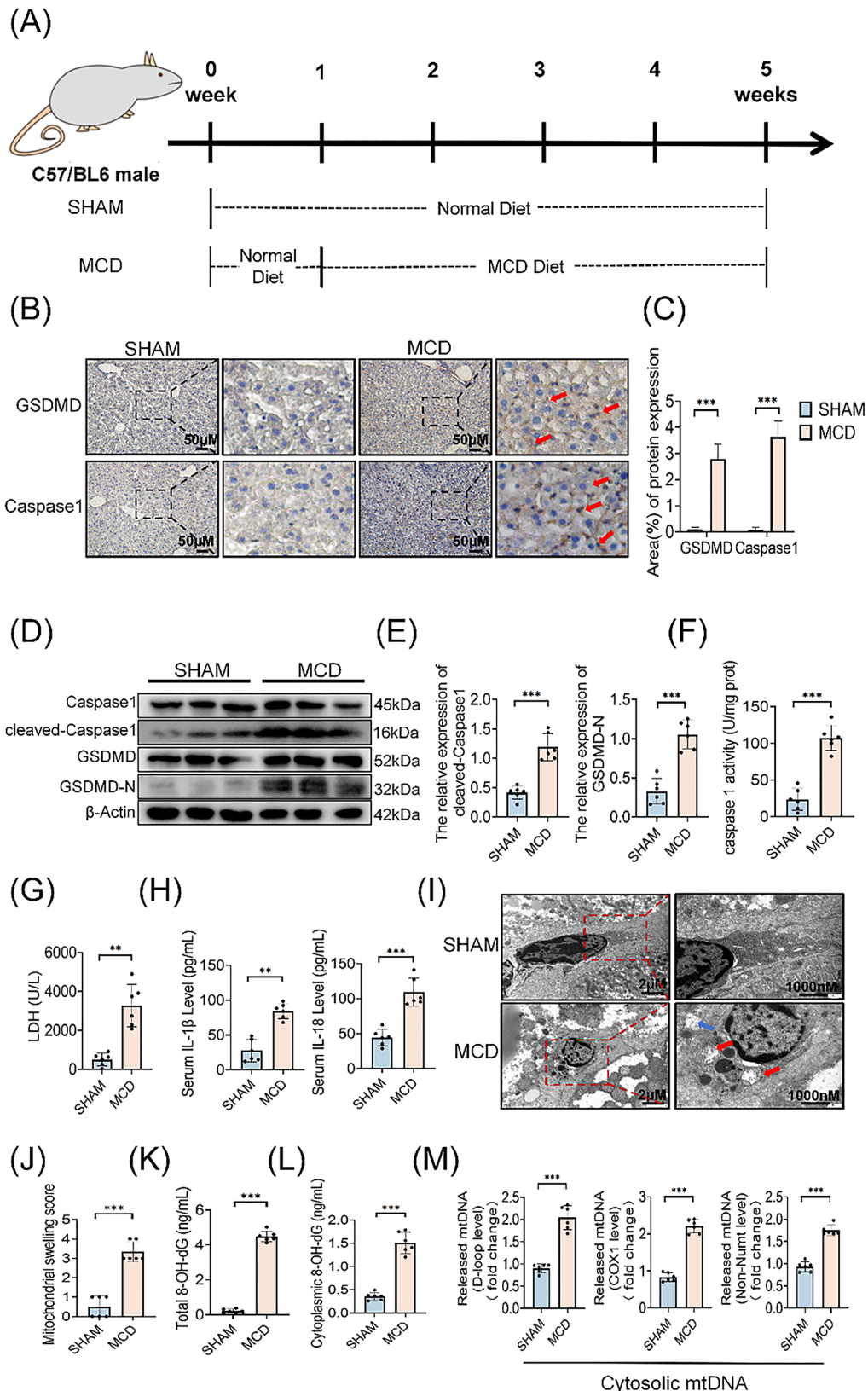
Statistical analysis

All data were analyzed using SPSS 18.0 (SPSS Inc., Chicago, USA). Normality was evaluated using the Shapiro-Wilk test, with $P>0.05$ indicating normal distribution. Normally distributed data are presented as mean \pm SD and analyzed by Student's t-test, while non-normally distributed data are expressed as median (range) and compared using the Mann-Whitney U test. Statistical significance was defined as $P<0.05$ for all tests.

Results

Macrophages in MCD animal model showed significant pyroptosis and Ox-mtDNA release

In order to explore the specific mechanism of Ox-mtDNA driving pyroptosis and MASH, we selected MCD to establish a model and verify the model results (Fig. S2. A-G), and carried out the following experiments. Figure 1. A is the mouse modeling process. IHC showed that the expression of Caspase1 and GSDMD (red arrows) in liver tissue in the MCD group was significantly increased (Fig. 1. B-C), indicating that pyroptosis occurred mainly in non-parenchymal cells (e.g., macrophages). WB experiments on our isolated primary liver macrophages showed that the levels of cleaved-Caspase1 and GSDMD-N proteins in the MCD group were significantly up-regulated (Fig. 1. D-E). Caspase1 activity and LDH were significantly upregulated (Fig. 1. F-G). The release of IL-1 β and IL-18 was increased in the MCD group by Elisa (Fig. 1. H). TEM showed typical pyroptosis morphological features of macrophages in the MCD group, including plasma membrane rupture (blue arrow) and mitochondrial swelling (red arrows) (Fig. 1. I). The

**Fig. 1** (See legend on next page)

(See figure on previous page.)

Fig. 1 Macrophages in MCD animal model showed significant pyroptosis and Ox-mtDNA release. Liver in mice were subjected to MCD or normal diet for 4 weeks: **A**, Schematic diagram of the animal experiment modeling process. **B-C**, GSDMD and Caspase1 were detected using IHC in liver tissue sections (scale bar, 50 μ M) and area (%) of protein expression. **D-E**, Liver macrophages in each group were isolated, and the levels of Caspase1, cleaved-Caspase1, GSDMD and GSDMD-N were measured by WB. **F**, Liver macrophages in each group were isolated, and Caspase1 activity was determined with the Caspase1 assay kit. **G**, Serum levels of LDH were measured. **H**, The levels of serum inflammatory factors (IL-1 β and IL-18) were tested by ELISA. **I-J**, TEM was used to observe the ultrastructural changes in macrophages (scale bar, 2 μ M and 100 nm) and mitochondrial swelling score. **K**, 8-OH-dG from total cell was quantified using the 8-OH-dG ELISA kit. **L**, 8-OH-dG from cytosol was quantified using the 8-OH-dG ELISA kit. Liver macrophages from normal mice and liver macrophages from MCD animal model were measured. **M**, Relative cytosolic mtDNA amounts in each group. The relative ratios of D-loop mtDNA, COX1 mtDNA, or Non-Numt mtDNA are tested by qPCR. All data are shown as the mean \pm SD ($n=6$). *** $P<0.001$, ** $P<0.01$ and * $P<0.05$

mitochondrial swelling score was significantly higher than that of the SHAM group (Fig. 1. J). Both total and intracellular 8-OH-DG levels increased (Fig. 1. K-L), suggesting oxidative damage to DNA in the cytoplasm. The levels of mitochondrial markers (D-loop, COX1, and Non-Numt) in the cytoplasm increased (Fig. 1. M). The above results suggest that the content of Ox-mtDNA in the cytoplasm is increased.

These results indicate that in MCD animal model, liver macrophages undergo significant pyroptosis, characterized by Caspase1/GSDMD activation, inflammatory factor release, and typical morphological changes.

Ox-mtDNA release may be a key factor in triggering pyroptosis in macrophages, thereby exacerbating inflammation and liver damage in MASH.

Blocking Ox-mtDNA release mitigates pyroptosis of macrophages and liver damage in MCD animal model

To determine whether Ox-mtDNA release promotes pyroptosis and MASH progression in macrophages, we used CsA to inhibit mitochondrial DNA release (Fig. 2. A). It was found through confocal microscopy that CsA does not cause damage to mitochondria (Fig. S2. H). In addition, we found that CsA significantly inhibited the release of Ox-mtDNA in liver macrophages (Fig. 2. B-C) (D-loop, COX1 and Non-Numt are mitochondrial markers). And CsA does not affect total Ox-mtDNA

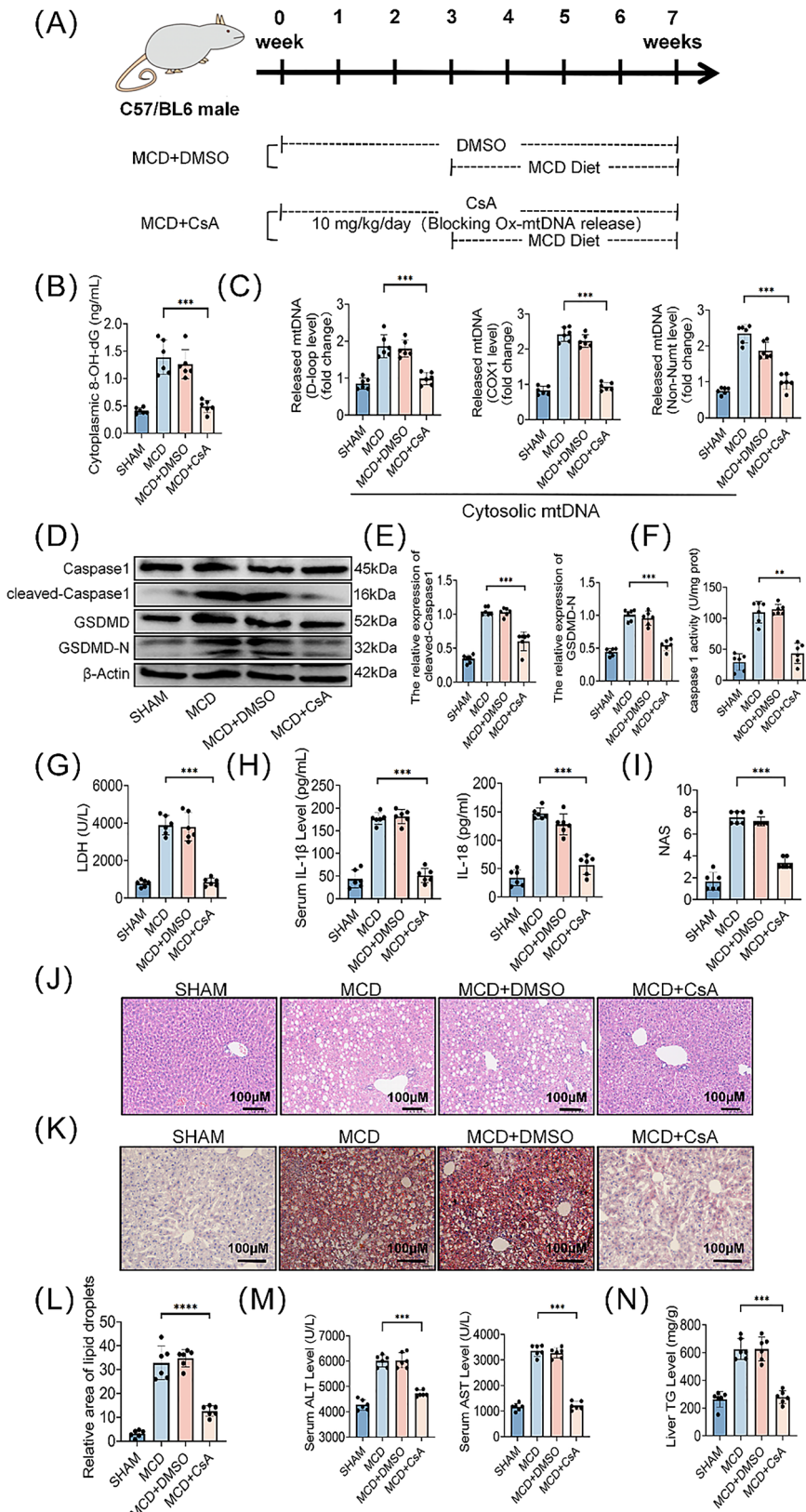
production (Fig. S2. I-J). WB showed that the expression of cleaved-Caspase1 and GSDMD-N proteins was up-regulated (Fig. 2. D-E). The Caspase1 activity was enhanced (Fig. 2. F). Also, LDH, IL-1 β , and IL-18 releases increased (Fig. 2. G-H). It was shown that the release of Ox-mtDNA was a key factor in triggering pyroptosis in macrophages.

H&E staining, NAS score, and oil red O staining (Fig. 2. I-L) showed that Inhibits Ox-mtDNA release significantly reduced liver injury and lipid droplets. Serum ALT and AST levels (Fig. 2. M) and liver TG (Fig. 2. N) were also significantly reduced.

These results suggest that inhibition of Ox-mtDNA release is effective in attenuating macrophage pyroptosis, thereby improving liver injury in MCD animal models.

FFA induces Ox-mtDNA release via mPTP, leading to pyroptosis of THP-1 derived macrophages

Using PMA to induce THP-1 derived macrophages adherence, and then add FFA to model it for 24 h. Oil red O staining showed a significant increase in lipid droplets in the FFA group compared with the CON (Fig. S3. A-B). Fluorescence detection showed that the mPTP channel was significantly opened after FFA stimulation (Fig. 3. A). To identify triggers for mPTP opening, we detected cytosolic ROS, as both ROS and calcium overload are thought to drive mPTP opening [22]. Flow cytometry confirmed

**Fig. 2** (See legend on next page.)

(See figure on previous page.)

Fig. 2 Blocking Ox-mtDNA release mitigates pyroptosis of macrophages and liver damage in MCD animal model. Mice were fed CsA10 mg/kg/day continuously for 7 weeks, and the MCD diet was started in the third week. Isolate each group of liver macrophages: **(A)** Schematic diagram of the feeding process of mice in each group. **(B)** 8-OH-dG in cytosol were quantified using ELISA. **(C)** Relative cytosolic mtDNA amounts in each group. The relative ratios of D-loop mtDNA, COX1 mtDNA, or Non-Numt mtDNA are tested by qPCR. **D-E** The levels of Caspase1, cleaved-Caspase1, GSDMD and GSDMD-N were measured by WB. **F**. Caspase1 activity was determined with the Caspase1 assay kit. **G**. Supernatant levels of LDH were measured by LDH assay kit. **H**. Supernatant levels of IL-1 β and IL-18 were tested by ELISA. **I-J**. NAS scores are based on H&E-stained liver sections (scale bars, 100 μ M) from different groups of mice. **K-L**. Oil red staining is based on liver sections (scale bar, 100 μ M) from different groups of mice and relative area of lipid droplets. **M-N**. Serum levels of ALT, AST and liver TG were measured by biochemical kit. All data are shown as the mean \pm SD ($n=6$). *** $P<0.001$, ** $P<0.01$ and * $P<0.05$

a significant increase in cytosolic ROS in the FFA group, however, DPI effectively cleared cytosolic ROS (Fig. S3. C). After DPI treatment, the mPTP channel was closed, indicating that the key trigger for its opening was cytosolic ROS (Fig. S3. D). We isolated THP-1 derived macrophage cytoplasm and mitochondria. Elisa, qPCR (human mitochondrial markers D-loopHV1, COX2, ND1), and fluorescence colocalization showed that the cytosolic Ox-mtDNA levels in the FFA group were significantly higher than those in the CON group (Fig. 3. B-D), indicating that excessive ROS-induced mPTP opening led to the release of Ox-mtDNA.

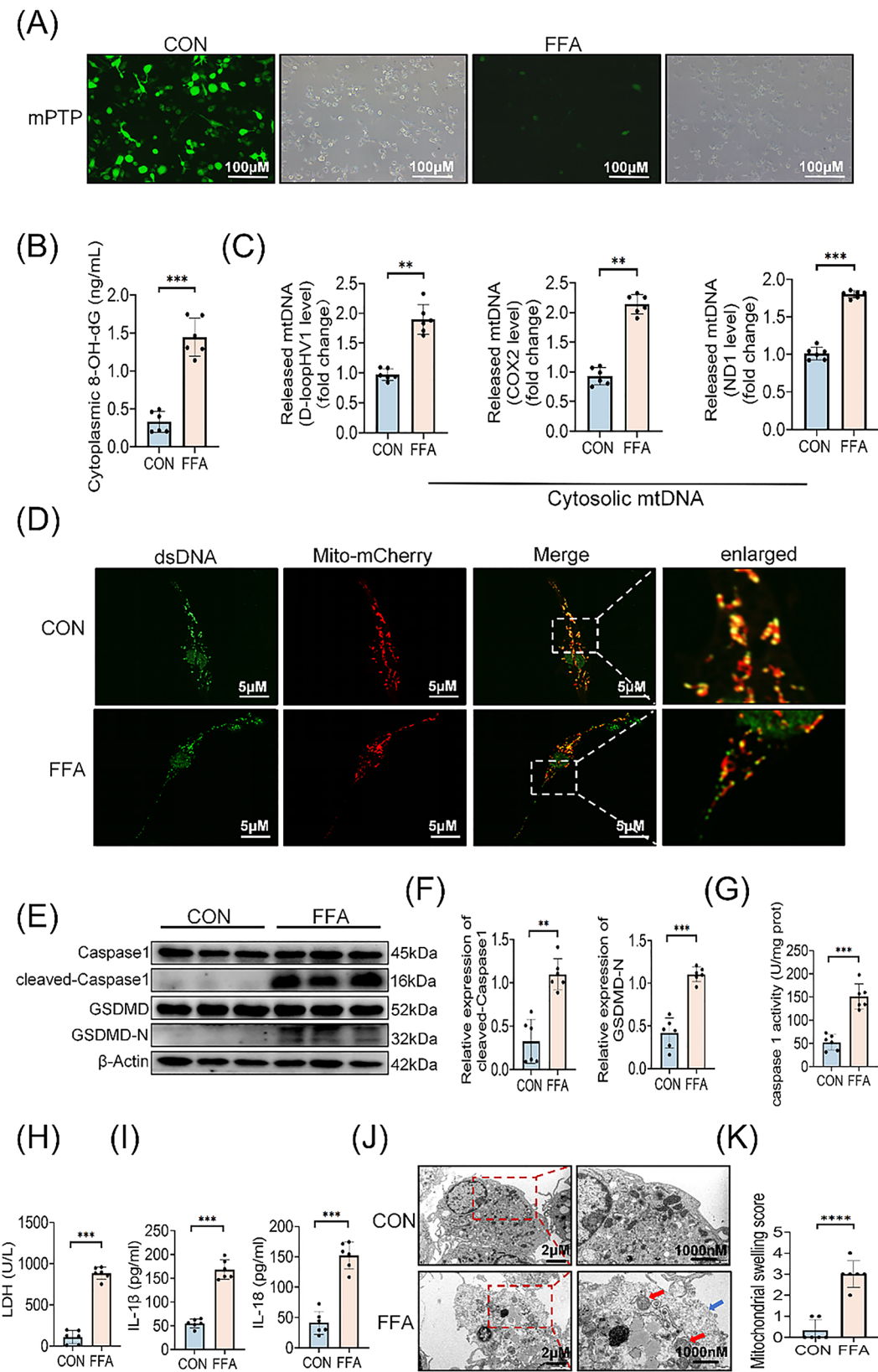
Pyroptosis-related indexes in the FFA group changed significantly: WB showed that the expression of cleaved-Caspase1 and GSDMD-N proteins was up-regulated (Fig. 3. E-F). Caspase1 activity was enhanced (Fig. 3. G); LDH, IL-1 β , and IL-18 release from cell supernatant increased (Fig. 3. H-I). TEM observations showed that the FFA group showed typical pyroptosis patterns: membrane pore formation (blue arrow), mitochondrial swelling (red arrows), etc. (Fig. 3. J), and the mitochondrial swelling score was increased (Fig. 3. K).

In conclusion, molecular and morphological evidence suggests that FFA can effectively induce pyroptosis in THP-1 derived macrophages.

Blocking Ox-mtDNA release attenuates THP-1 derived

macrophages pyroptosis and reduces lipid droplets in vitro

To elucidate the role of cytosolic Ox-mtDNA on pyroptosis in macrophages, we used CsA to block Ox-mtDNA release. As shown in Fig. 4. A, where CsA significantly inhibited mPTP channel opening compared to the FFA group. Elisa and qPCR showed that FFA stimulation resulted in the release of Ox-mtDNA into the cytoplasm, but in the FFA + CsA group, cytosolic Ox-mtDNA was significantly reduced (human mitochondrial markers D-loopHV1, COX2, ND1) (Fig. 4. B-C). In addition, immunofluorescence staining showed that CsA significantly enhanced the colocalization of mtDNA with mitochondria (Fig. 4. D), indicating that CsA effectively limited cytoplasmic translocation of Ox-mtDNA. WB analysis revealed that inhibiting Ox-mtDNA release significantly attenuated FFA-induced cleaved-Caspase1 and GSDMD-N expression (Fig. 4. E-F). At the same time, the Caspase1 activity assay showed a significant decrease in the CsA group (Fig. 4. G). Analysis of cell culture supernatants showed that FFA stimulation resulted in a significant increase in the release of LDH, IL-1 β , and IL-18, after inhibiting the release of Ox-mtDNA, the release decreased (Fig. 4. H-I). Macrophage pyroptosis is further confirmed. TEM confirmed that the CsA group cells

**Fig. 3** (See legend on next page.)

(See figure on previous page.)

Fig. 3 FFA induces Ox-mtDNA release via mPTP, leading to pyroptosis of THP-1 derived macrophages. THP-1 derived macrophages were cultured for 24 h with normal or FFA added. **(A)** Representative of immunofluorescence staining of Calcein (green) and corresponding cell density (white light). **(B)** 8-OH-dG in cytosol were quantified using ELISA. **(C)** Relative cytosolic mtDNA amounts in each group. The relative ratios of D-loopHV1 mtDNA, COX2 mtDNA, or ND1 mtDNA are tested by qPCR. **(D)** The colocalization of Mito-mCherry (red) and dsDNA (green) was detected by confocal microscopy. **E-F**. The levels of Caspase1, cleaved-Caspase1, GSDMD and GSDMD-N were measured by WB. **G**. Caspase1 activity was determined with the Caspase1 assay kit. **H**. Supernatant levels of LDH were measured by LDH assay kit. **I**. Supernatant levels of IL-1 β and IL-18 were tested by ELISA. **J-K**. TEM was used to observe the ultrastructural changes in macrophages (scale bar, 2 μ m and 100 nm) and mitochondrial swelling score. All data are shown as the mean \pm SD ($n=6$). *** $P<0.001$, ** $P<0.01$ and * $P<0.05$

exhibited improved morphology, characterized by preservation of membrane integrity (blue arrow) and reduced mitochondrial swelling (red arrow) (Fig. 4. J-K). Additionally, Oil Red O staining demonstrated that inhibiting Ox-mtDNA release significantly alleviated FFA-induced lipid droplets (Fig. 4. L-M).

Collectively, these findings indicate that inhibiting Ox-mtDNA release not only mitigates FFA-induced THP-1 derived macrophages pyroptosis but also ameliorates lipid droplets within the cytoplasm.

Ox-mtDNA activates NLRP3 by regulating the release of Ca²⁺ from ITPR3 channels

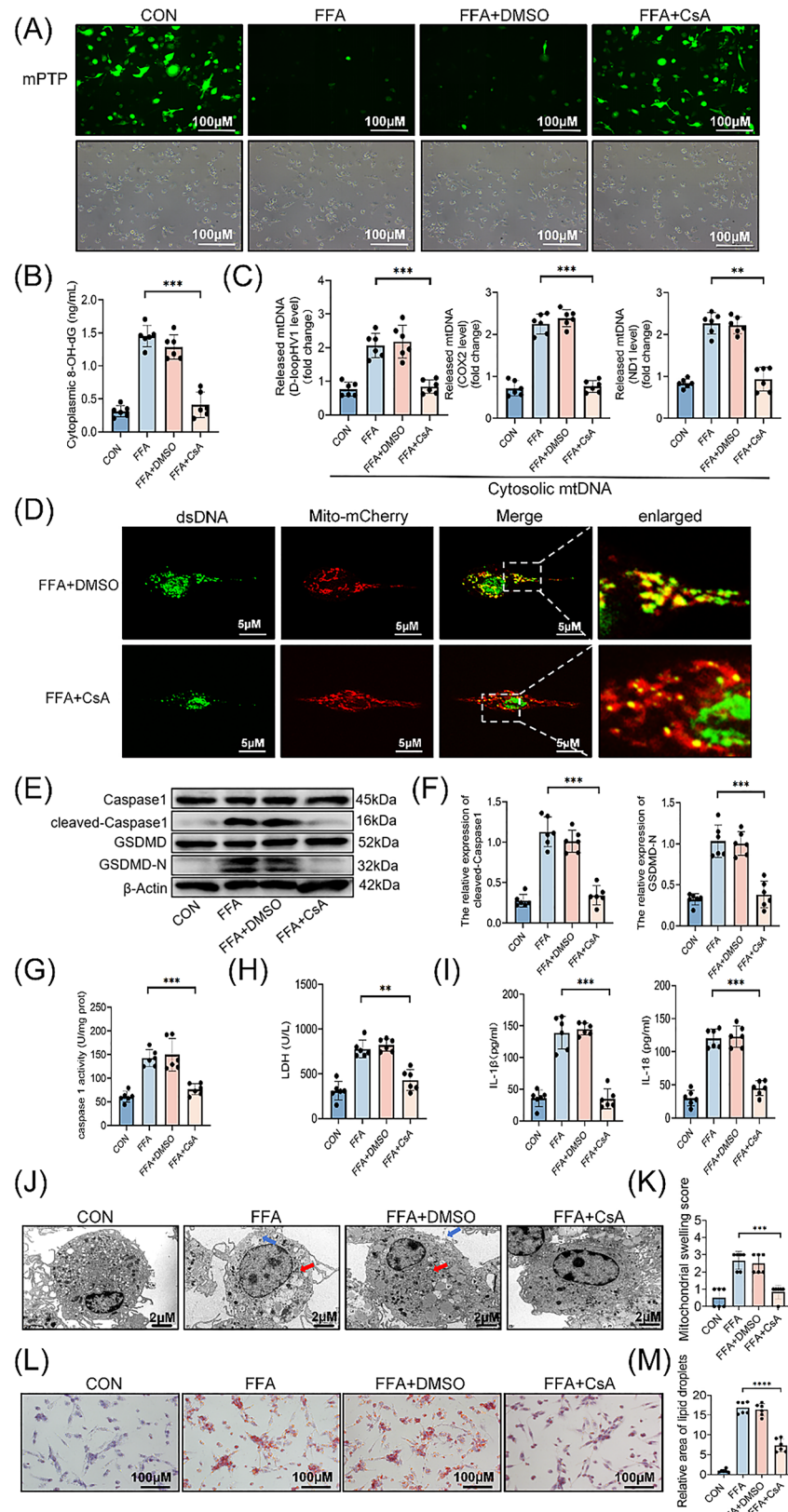
RNA-seq analysis of THP-1 derived macrophages treated with FFA or FFA + CsA showed that there were 556 significant up-regulation genes ($\log_{2}FC \geq 1$, $p < 0.05$) and 668 down-regulation genes ($\log_{2}FC \leq -1$, $p < 0.05$) (Fig. 5. A). According to gene ontology (GO) analysis, differentially expressed genes (DEGs) were significantly enriched in the calcium-related pathway (Fig. 5. B). Kyoto Encyclopedia Gene and genome (KEGG) enrichment analysis was associated with NOD pathway (Fig. 5. C), ITPR3 was significantly enriched in the NOD pathway (Fig. 5. D). The heat map showed that ITPR3 was significantly down-regulated in the FFA + CsA group compared to the FFA group (Fig. 5. D). Given that ITPR3 is a key channel protein for the release of Ca²⁺ on the ER, it can activate NLRP3 inflammasomes [33, 34]. Therefore, ITPR3/Ca²⁺/NLRP3 may be a key mechanism by which Ox-mtDNA promotes pyroptosis in macrophages.

Next, based on the RNA-seq we performed the following validation: the mRNA level of ITPR3 was verified by qPCR (Fig. 5. E). WB analysis showed that FFA significantly increased the expression of ITPR3, but blocking the release of Ox-mtDNA decreased the expression of ITPR3 (Fig. 5. F-G). Notably, while the RNA-seq did not show changes in NLRP3 mRNA levels (Fig. 5. D), WB showed that FFA significantly enhanced NLRP3 expression (Fig. 5. F-G), suggesting that Ox-mtDNA may regulate NLRP3 at post-translational levels. Next, immunofluorescence showed that the expression of ITPR3 and NLRP3 was significantly reduced after inhibiting the release of Ox-mtDNA compared with the FFA group (Fig. 5. H). Fluo-4 AM Ca²⁺ imaging confirmed that intracellular Ca²⁺ concentrations were significantly increased in FFA-treated cells, and this phenomenon was effectively inhibited by inhibition of Ox-mtDNA release (Fig. 5. I).

It has been shown that the release of ox-mtDNA promotes the expression of ITPR3 and NLRP3, and the level of intracellular Ca²⁺.

Inhibition of ITPR3/Ca²⁺ axis alleviates NLRP3-dependent pyroptosis in liver macrophages and reduces the intracellular lipid droplets

Next, we further validate the mechanism in vitro. We successfully knocking down ITPR3 in THP-1 derived macrophages (Fig. S4. A), we restored intracellular Ca²⁺ levels using a Ca²⁺ carrier (Ionomycin: Iono) to verify the role of the ITPR3/Ca²⁺ pathway in pyroptosis.

**Fig. 4** (See legend on next page)

(See figure on previous page.)

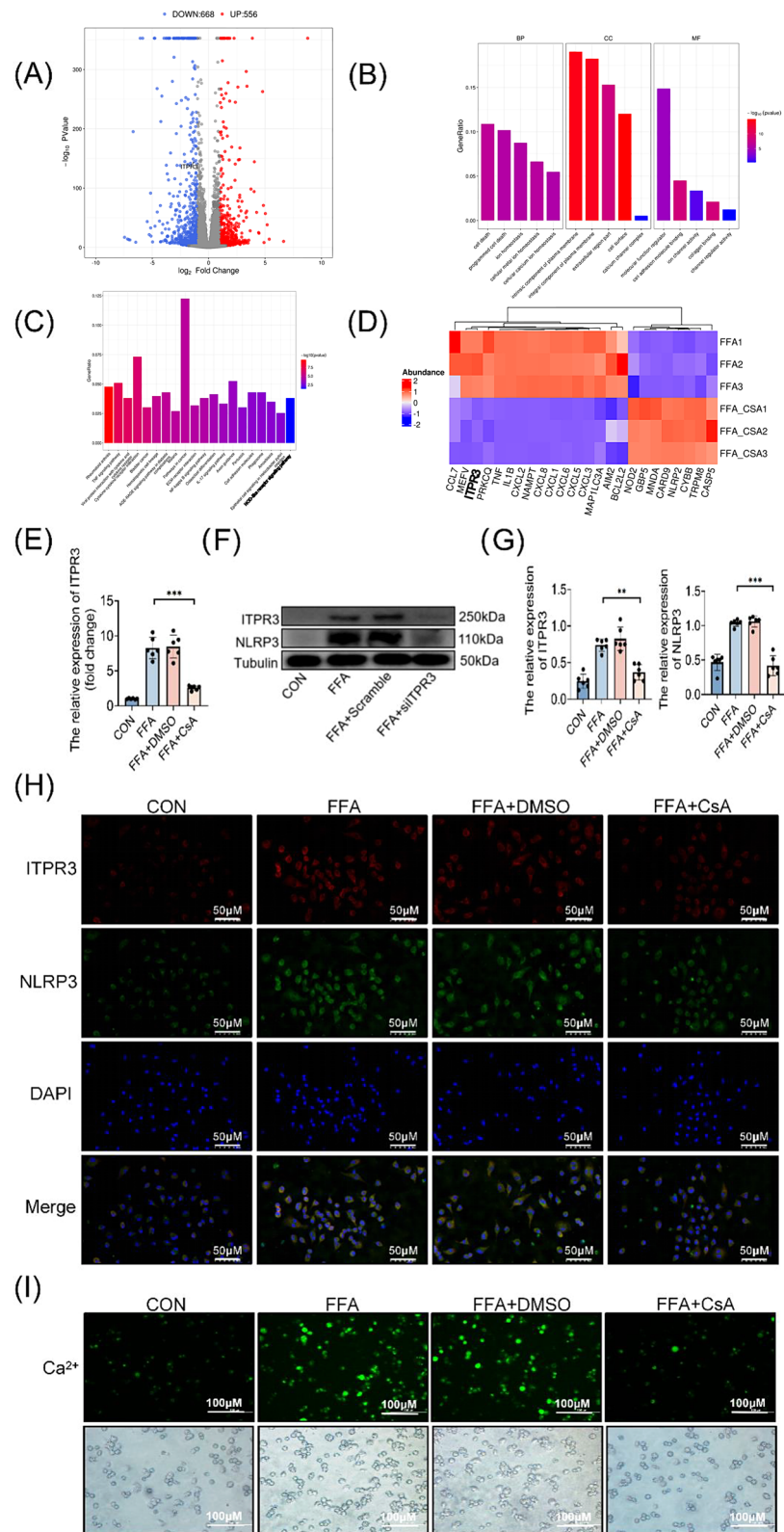
Fig. 4 Blocking Ox-mtDNA release attenuates THP-1 derived macrophages pyroptosis and reduces lipid droplets in vitro. In the absence or presence of CsA (1 μ M), THP-1 derived macrophages were cultured normally as well as FFA/DMSO added. **(A)** Representative of immunofluorescence staining of Calcein (green) and corresponding cell density (white light). **(B)** 8-OH-dG in cytosol were quantified using ELISA. **(C)** Relative cytosolic mtDNA amounts in each group. The relative ratios of D-loopHV1 mtDNA, COX2 mtDNA, or ND1 mtDNA are tested by qPCR. **(D)** The colocalization of Mito-mCherry (red) and dsDNA (green) was detected by confocal microscopy. **E-F.** The levels of Caspase1, cleaved-Caspase1, GSDMD and GSDMD-N were measured by WB. **G.** Caspase1 activity was determined with the Caspase1 assay kit. **H.** Supernatant levels of LDH were measured by LDH assay kit. **I.** Supernatant levels of IL-1 β and IL-18 were tested by ELISA. **J-K.** TEM was used to observe the ultrastructural changes in macrophages (scale bar, 2 μ M) and mitochondrial swelling score. **L-M.** Oil red staining is based on each group of cells and relative area of lipid droplets. All data are shown as the mean \pm SD ($n=6$). *** $P<0.001$, ** $P<0.01$ and * $P<0.05$.

Fluorescence results showed that ITPR3-siRNA down-regulated intracellular Ca²⁺ levels, however, intracellular Ca²⁺ levels increased after Iono treatment (Fig. 6. A). The WB results showed that ITPR3-siRNA reduced the expression levels of ITPR3, NLRP3 and other pyroptosis-related indicators (Fig. 6. D-H). However, after the increase of intracellular Ca²⁺, the expression of NLRP3 increased (Fig. 6. B-C), and the expression of pyroptosis-related indicators increased (Fig. 6. D-H). TEM results showed that knockdown of ITPR3 reduced the occurrence of pyroptosis: membrane rupture (blue arrow) and mitochondrial swelling (red arrow), which was exacerbated by increased intracellular Ca²⁺ (Fig. 6. I-J). In addition, oil red O staining showed that ITPR3 knockdown significantly attenuated FFA-induced lipid droplets, while restoring intracellular Ca²⁺ increased lipid droplets compared to the knockdown group, but not as much as in the FFA group (Fig. 6. K-L).

These results conclusively demonstrate that the ITPR3/Ca²⁺/NLRP3 signaling axis serves as a crucial regulatory mechanism for Ox-mtDNA mediated macrophage pyroptosis.

Inhibition of ITPR3/Ca²⁺ signaling blocks Ox-mtDNA induced liver macrophages pyroptosis and mitigates MCD animal model damage

To confirm the above conclusions *in vivo*, we specifically knocked out ITPR3 of liver macrophages by injecting adeno-associated virus into the tail of mice (Fig. 7. A) and verified (Fig. S4. B). WB analysis revealed that compared to the MCD group, the ITPR3-AAV group exhibited significantly reduced expression of ITPR3, NLRP3, cleaved-Caspase1, and GSDMD-N (Fig. 7. B-E). Functional assays demonstrated that ITPR3-AAV group markedly decreased Caspase1 activity (Fig. 7. F) and reduced serum levels of LDH, IL-1 β , and IL-18 (Fig. 7. G-H). TEM analysis (Fig. S4. C) Macrophage morphology was improved in the ITPR3-AAV group, characterized by normal membrane integrity (blue arrow) and organelle structure (red arrow). At the same time, mitochondrial swelling was significantly reduced after specific knockdown of ITPR3 (Fig. S4. D). H&E staining and Oil Red O staining further confirmed that ITPR3 knockout effectively alleviated FFA-induced liver injury and intracellular lipid droplets (Fig. 7. I-J). Serum biochemical assays

**Fig. 5** (See legend on next page.)

(See figure on previous page.)

Fig. 5 Ox-mtDNA activates NLRP3 by regulating the release of Ca^{2+} from ITPR3 channels. In the absence or presence of CsA (1 μM), RNA-seq experiments are performed 24 h after FFA stimulation of THP-1 derived macrophages: **(A)** Volcano map of differential genes. **(B)** GO enrichment analysis showed a high correlation with calcium. **(C)** KEGG shows correlation with the NOD pathway. **(D)** The heatmap showed the difference in the expression of ITPR3 in the NOD pathway. **(E)** The expression level of ITPR3 mRNA was detected by qPCR. **F-G.** The levels of ITPR3 and NLRP3 were measured by WB. **H.** Intracellular ITPR3 and NLRP3 expression were measured by immunofluorescence. **I.** The Fluo4 series calcium fluorescence indicator kit measures the concentration of Ca^{2+} in the cytosol and the corresponding cell density (white light). All data are shown as the mean \pm SD ($n=6$). *** $P<0.001$, ** $P<0.01$ and * $P<0.05$

showed that macrophage-specific ITPR3 deletion significantly reduced ALT and AST levels (Fig. 7. K), and liver TG levels (Fig. 7. L).

These in vivo results conclusively suggest that Ox-mtDNA promotes pyroptosis in liver macrophages by activating the ITPR3/ Ca^{2+} /NLRP3 signaling pathway, thereby exacerbating MCD-induced MASH progression (Fig. 8). This issue is likely to provide a new potential therapeutic target for MASH.

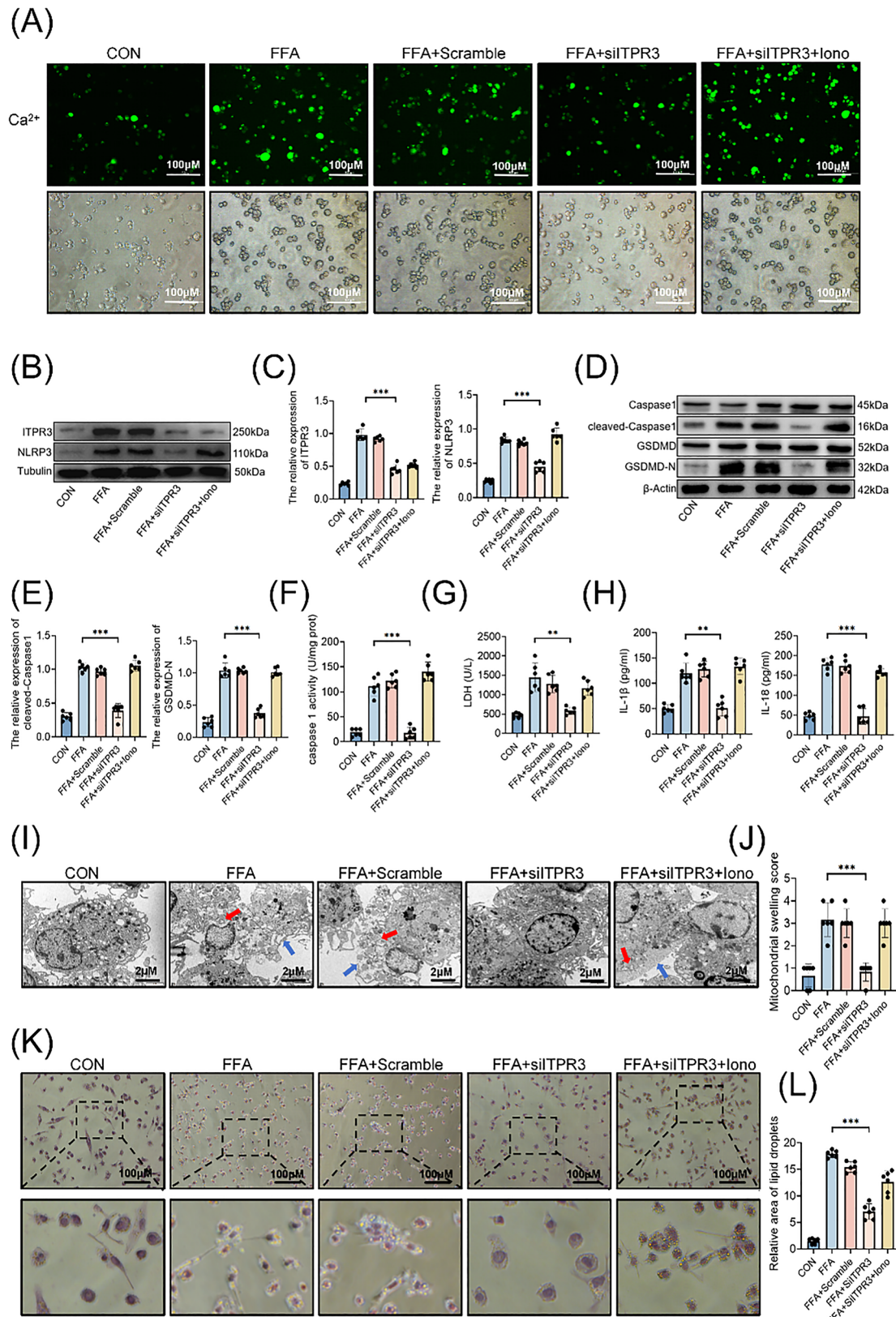
Discussion

In this study, we reported a discovery that Ox-mtDNA is released into the cytoplasm through mPTP channels in macrophages during MCD-induced MASH. More importantly, a new mechanism was elucidated by which cytosolic Ox-mtDNA triggers the ITPR3/ Ca^{2+} /NLRP3 signaling pathway to mediate macrophage pyroptosis and exacerbate MCD-induced MASH.

MCD mice showed significant inflammation at week 4. However, the HFD-fed mice fed for 8 weeks showed only mild inflammation and fibrosis, and by week 16, the HFD-fed mice showed a significant increase in inflammation and fibrosis, highlighting the different progression patterns of liver pathology in the HFD model [35]. At the same time, HFD-fed mice only showed a large of lipid droplets at week 8 [36], while we found that mice

fed MCD had a large of lipid droplets at week 4. For in vivo experiments, An MCD diet is a classic method to induce MASH in animal models. MCD diets promote the dysfunction of liver mitochondrial β -oxidation, thereby establishing an animal model of MASH [37]. This model is mainly used to study inflammation, oxidative stress, mitochondrial damage, and liver fibrosis related to MASH [38, 39]. This model has the advantages of a short modeling time, little influence by individual differences, and good uniformity and stability of liver inflammation [39].

In FFA-induced THP-1 derived macrophage models, we observed significant accumulation of cytosolic Ox-mtDNA, which is consistent with the mitochondrial DNA release mechanism associated with impaired mitochondrial quality control [40, 41]. It is interesting that the accumulation of Ox-mtDNA has different biological significance in the bloodstream and cytoplasm. Circulatory Ox-mtDNA predominantly resides in extracellular fluids (e.g., blood), functioning as both a systemic inflammatory mediator and clinical biomarker that reflects tissue damage severity [12, 42]. Cytosolic Ox-mtDNA localizes to the cytosol where it acts as a direct effector molecule of metabolic stress, participating in cell-autonomous immune regulation [13]. These two forms demonstrate functional complementarity: circulatory Ox-mtDNA provides diagnostic utility for clinical evaluation, while

**Fig. 6** (See legend on next page.)

(See figure on previous page.)

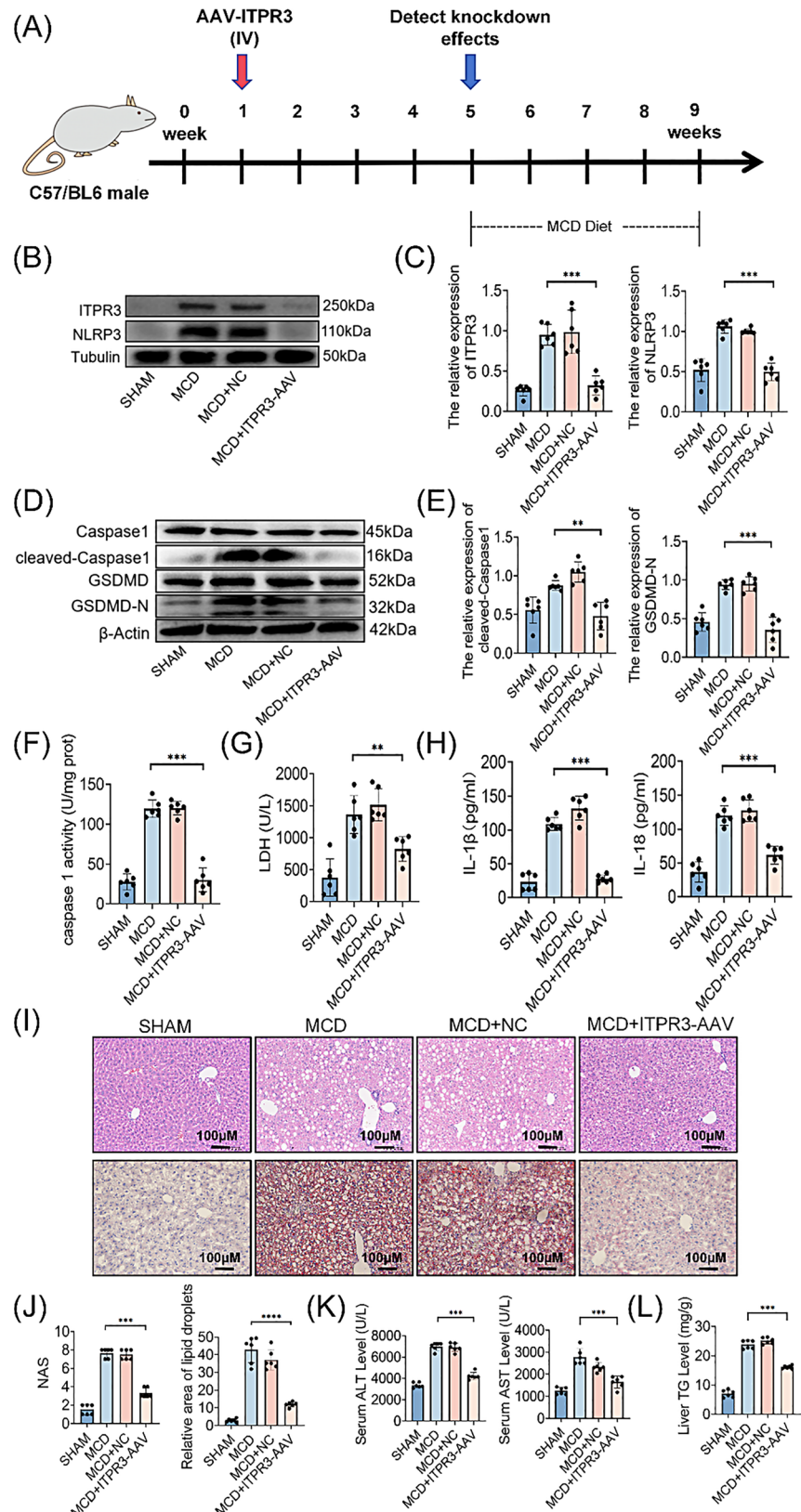
Fig. 6 Inhibition of ITPR3/Ca²⁺ axis alleviates NLRP3-dependent pyroptosis in liver macrophages and reduces the intracellular lipid droplets. Treat THP-1 derived macrophages with si-ITPR3/Scramble/lono, cultured with normal or FFA for 24 h: **A**, The Fluo4 series calcium fluorescence indicator kit measures the concentration of Ca²⁺ in the cytosol and the corresponding cell density (white light). **B-E**, The levels of ITPR3, NLRP3, Caspase-1, cleaved-Caspase1, GSDMD and GSDMD-N were measured by WB. **F**, Caspase1 activity was determined with the Caspase1 assay kit. **G**, Supernatant levels of LDH were measured by LDH assay kit. **H**, Supernatant levels of IL-1 β and IL-18 were tested by ELISA. **I-J**, TEM was used to observe the ultrastructural changes in macrophages (scale bar, 2 μ M) and mitochondrial swelling score. **K-L**, Oil red staining is based on each group of cells and relative area of lipid droplets. All data are shown as the mean \pm SD ($n=6$). *** $P<0.001$, ** $P<0.01$ and * $P<0.05$

intracellular Ox-mtDNA serves as a mechanistic research target [14].

Mitochondrial DNA can be released into the cytoplasm through mPTP channels or BAX/BAK pores [43, 44]. Among them, the mPTP channel mainly releases oxidatively damaged mtDNA (Ox-mtDNA), which is produced by ROS attack [22, 42]. And the mtDNA released by BAX/BAK pores is mainly related to apoptosis [44]. Notably, our study confirms that targeted intervention of mPTP channels reduces Ox-mtDNA release and improves macrophage pyroptosis and MCD-induced MASH. This further provides direct evidence for therapeutic strategies for Ox-mtDNA release.

Our RNA-seq showed that the mRNA level of ITPR3 was significantly upregulated in FFA induced THP-1 derived macrophages, while the mRNA level of ITPR3 was downregulated after CsA inhibited Ox mtDNA release. Subsequent experiments have confirmed that the expression of ITPR3 protein is consistent with changes in mRNA levels. In addition, FFA induced a significant increase in intracellular Ca²⁺ levels in THP-1 derived macrophages, while inhibition of Ox mtDNA release or ITPR3 knockout significantly reduced intracellular Ca²⁺ levels. In fact, recent research findings indicate

that changes in ITPR subtype expression are associated with various human diseases, from fatty liver to cancer, ITPR3 is emerging as the isoform that is particularly important in the pathogenesis of various human diseases [45]. According to relevant literature reports, the ITPR3/Ca²⁺ axis can mediate apoptosis [46], and in addition, it can reduce the Ca²⁺ concentration in the cytoplasm and mitochondria, thereby inhibiting macrophage M1 polarization [47]. However, our discovery of the ITPR3/Ca²⁺ signaling pathway provides new insights into the mechanism of NLRP3 inflammasome activation. Previous studies have shown that mitochondrial DNA induces pyroptosis in nucleus pulposus cells via the TLR9-NF- κ B-NLRP3 axis [29, 48], but our study reveals a novel ITPR3-mediated Ca²⁺ signaling axis that activates NLRP3 and thus promotes macrophage pyroptosis and MASH. Ca²⁺ signaling plays a key role in the activation of NLRP3 inflammasomes in liver macrophages [49, 50]. Ca²⁺ acts as a second messenger, activating the downstream effector CaMKII, which subsequently synergistically amplifies the storm of pro-inflammatory factors such as TNF- α and IL-1 β by phosphorylating key molecules of the NF- κ B pathway (e.g., P65) and enhancing NLRP3 activity, thereby promoting the inflammatory response in the

**Fig. 7** (See legend on next page.)

(See figure on previous page.)

Fig. 7 Inhibition of ITPR3/Ca²⁺ signaling blocks Ox-mtDNA induced liver macrophages pyroptosis and mitigates MCD animal model damage. The mice in the experimental group were injected with ITPR3-AAV through the tail vein: **A**. Schematic diagram of animal experiments. **B-E**. The levels of ITPR3, NLRP3, Caspase-1, cleaved-Caspase1, GSDMD and GSDMD-N were measured by WB. **F**. Caspase1 activity was determined with the Caspase1 assay kit. **G**. Supernatant levels of LDH were measured by LDH assay kit. **H**. Supernatant levels of IL-1 β and IL-18 were tested by ELISA. **I-J**. NAS score and lipid droplets relative area analysis were based on liver slice H&E staining and oil red staining (scale bar, 100 μ M) of different groups of mice. **K-L**. Serum levels of ALT, AST and liver TG were measured by biochemical kit. All data are shown as the mean \pm SD ($n=6$). *** $P<0.001$, ** $P<0.01$ and * $P<0.05$

brain [51]. In addition, the pathological effects of Ca²⁺ go far beyond that. NFAT family (especially NFATc1/c3), as downstream targets of Ca²⁺, is mediated by calcineurin, and NFATc1 signaling drives chronic ER stress response and promotes MASLD progression [52].

This study has important theoretical and clinical implications. The elucidated Ox-mtDNA-ITPR3/Ca²⁺/NLRP3 axis complements the popular “multiple hit” theory of MASLD pathogenesis [53, 54]. Also, we demonstrated that release of Ox-mtDNA is a key target for the treatment of MASLD, providing a theoretical basis for clinical treatment; Macrophage Ox-mtDNA, ITPR3, Ca²⁺ and pyroptosis are expected to be markers to assess the degree of inflammation in liver disease. These findings not only deepen the understanding of the pathogenesis of MASLD,

but also provide a theoretical basis for Ox-mtDNA targeted therapy.

However, despite some progress in our research, there are still important limitations in this study: How Ox-mtDNA directly interacts with ITPR3 and the specific signaling molecules involved in this process need to be studied more deeply; Although CsA is a classic mPTP inhibitor, its inhibitory effect on calcineurin may lead to off-target effects; Challenges such as AAV delivery and potential side effects also need to be addressed. This study lacks long-term observation of the progression of MASLD, and it is also necessary to further explore the results of different patient groups. The above limitations limit its potential for clinical translation, and in the future, we will explore these limitations in depth.

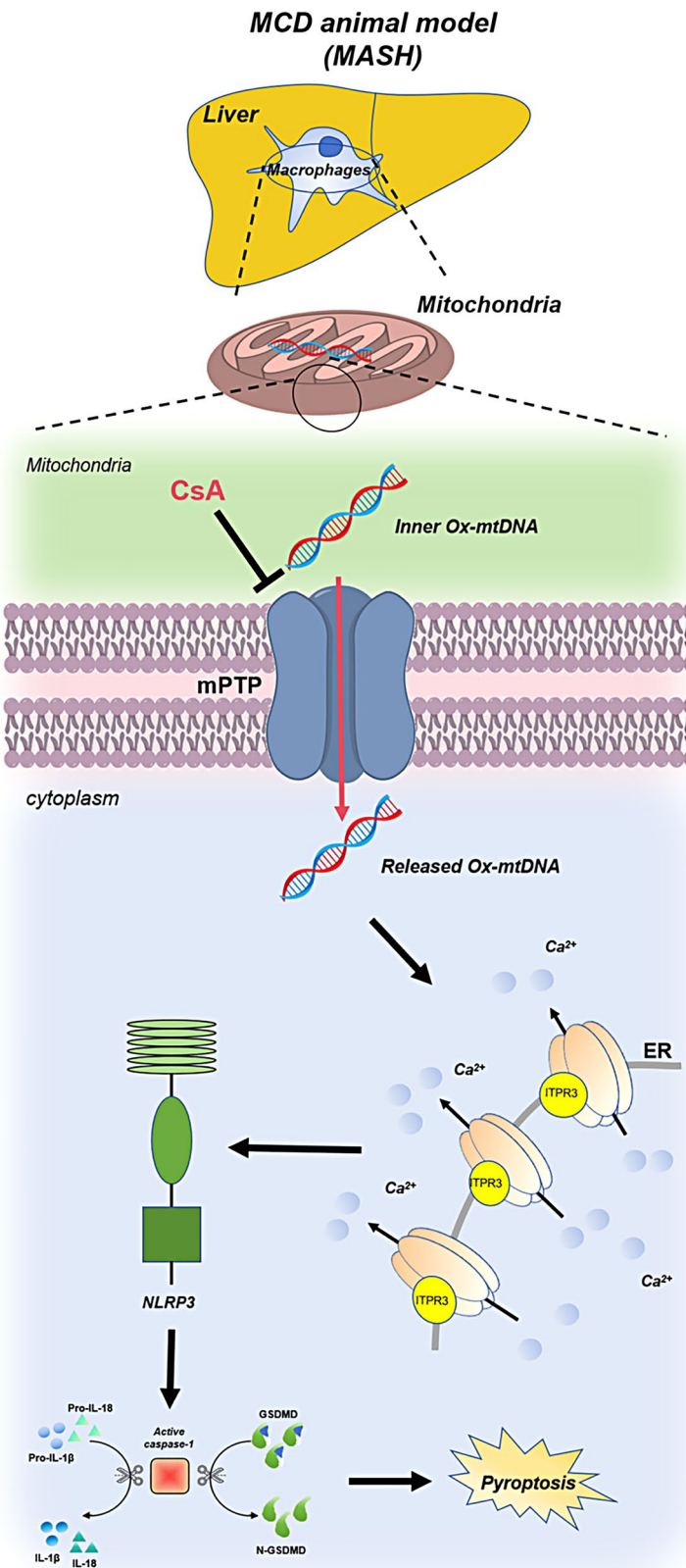


Fig. 8 Article mechanism diagram

Abbreviations

ALT	Aspartate transaminase
AST	Alanine aminotransferase
TG	Triglyceride
MCD	Methionine- and choline deficient diet
HFD	High-fat diet
ER	Endoplasmic reticulum
ROS	Reactive oxygen species
CsA	Cyclosporin A
Ca ²⁺	Calcium ions
GSDMD	Gasdermin D
LDH	Lactate dehydrogenase
mPTP	Mitochondrial permeability transition pore
Ox-mtDNA	Oxidized mitochondrial DNA
TEM	Transmission electron microscopy
ITPR3/IP3R	Inositol 1,4,5-Triphosphate Receptor Type 3
NLRP3	Nucleotide-binding domain and leucine-rich repeat protein-3
MASH	Metabolic Dysfunction-Associated Steatohepatitis
MASLD	Metabolic Dysfunction-Associated Steatotic Liver Disease
8-OH-dG	8-hydroxy-2'-deoxyguanosine
PMA	Phorbol 12-myristate 13-acetate
DPI	Diphenyleneiodonium chloride
ER	Endoplasmic reticulum
IL-1β/IL-18	Interleukin - 1β/interleukin 18
NK Cells	Natural Killer Cells
ILC1	Type 1 Congenital Lymphoid Cells
IFN-γ	Interferon-gamma
TNF-α	Tumor Necrosis Factor-alpha
NETs	Neutrophil extracellular traps
AMPs/DAMPs	Pathogen-associated molecular patterns/damage-associated molecular patterns
RT	Room temperature

Supplementary Information

The online version contains supplementary material available at <https://doi.org/10.1186/s12967-025-07302-8>.

Supplementary Material 1

Supplementary Material 2

Supplementary Material 3

Supplementary Material 4

Acknowledgements

None.

Author contributions

All authors have approved the final manuscript, and conformed to the guidelines as set out in the International Committee of Medical Journal Editors (ICMJE). Sheng-Wei Li and Xin-Yi Wu designed the study, supervised the project, revised article and approved the final version of the manuscript. Qi Zhang was responsible for acquisition of data and writing original draft. Li Chen was responsible for resource preparation, interpretation of data, and drafting partial content. Rui Wang, Jun-Yan Liu and Tao Liu were responsible for data curation and drafting partial content. analyzed the data and wrote partial content.

Funding

This research was funded by Natural Science Foundation of Chongqing Municipality (Number: CSTB2022NSCQ-MSX0091).

Data availability

All data included in this study are available upon request by contacting the corresponding author.

Declarations**Ethics approval and consent to participate**

Humane care guided by the guidelines of the National Institutes of Health was provided to all animals. All mice were raised under specific pathogen-free conditions, following the procedures approved by the Animal Use and Ethics Committee of the 2nd Affiliated Hospital of Chongqing Medical University.

Consent for publication

All authors agree to the publication of the article.

Competing interests

The authors declare that the research was conducted in the absence of any commercial or financial relationships that could be construed as a potential conflict of interest.

Author details

¹Department of Hepatobiliary Surgery, The Second Affiliated Hospital of Chongqing Medical University, Chongqing, China

²Clinical Medicine and Surgery, The First Affiliated Hospital of Dali University, Yunnan, China

³Rehabilitation Medicine, The Second Affiliated Hospital of Chongqing Medical University, Chongqing, China

Received: 13 May 2025 / Accepted: 11 October 2025

Published online: 14 November 2025

References

- Wang X, Zhang L, Dong B. Molecular mechanisms in MASLD/MASH-related HCC. *Hepatology*. 2024.
- EASL-EASD-EASO Clinical practice guidelines on the management of metabolic dysfunction-associated steatotic liver disease (MASLD). *Obes Facts*, 2024;17(4):374–444.
- Wu Q, et al. The microenvironment in the development of MASLD-MASH-HCC and associated therapeutic in MASH-HCC. *Front Immunol*. 2025;16:1569915.
- Tincopa MA, Anstee QM, Loomba R. New and emerging treatments for metabolic dysfunction-associated steatohepatitis. *Cell Metab*. 2024;36(5):912–26.
- Luci C, et al. Chronic inflammation in Non-Alcoholic steatohepatitis: molecular mechanisms and therapeutic strategies. *Front Endocrinol (Lausanne)*. 2020;11:597648.
- Torabizadeh M, et al. The association of nasal and blood eosinophils with serum IgE level in allergic rhinitis and asthma: A Case-Control study. *Health Sci Rep*. 2024;7(11):e70191.
- Remmerie A, Martens L, Scott CL. Macrophage subsets in Obesity, aligning the liver and adipose tissue. *Front Endocrinol (Lausanne)*. 2020;11:259.
- Luci C, et al. Natural killer cells and type 1 innate lymphoid cells are new actors in Non-alcoholic fatty liver disease. *Front Immunol*. 2019;10:1192.
- Tosello-Trampont AC, et al. NKp46(+) natural killer cells attenuate metabolism-induced hepatic fibrosis by regulating macrophage activation in mice. *Hepatology*. 2016;63(3):799–812.
- Herrero-Cervera A, Soehnlein O, Kenne E. Neutrophils in chronic inflammatory diseases. *Cell Mol Immunol*. 2022;19(2):177–91.
- Kazankov K, et al. The role of macrophages in nonalcoholic fatty liver disease and nonalcoholic steatohepatitis. *Nat Rev Gastroenterol Hepatol*. 2019;16(3):145–59.
- Raufi A, et al. Macrophages in graft-versus-host disease (GVHD): dual roles as therapeutic tools and targets. *Clin Exp Med*. 2025;25(1):73.
- Wang X, et al. Prolonged hypernutrition impairs TREM2-dependent effec-tocytosis to license chronic liver inflammation and NASH development. *Immunity*. 2023;56(1):58–e7711.
- Tacke F, et al. An integrated view of anti-inflammatory and antifibrotic targets for the treatment of NASH. *J Hepatol*. 2023;79(2):552–66.
- Gaul S, et al. Hepatocyte pyroptosis and release of inflammasome particles induce stellate cell activation and liver fibrosis. *J Hepatol*. 2021;74(1):156–67.
- Mridha AR, et al. NLRP3 inflammasome Blockade reduces liver inflammation and fibrosis in experimental NASH in mice. *J Hepatol*. 2017;66(5):1037–46.
- Xiang Q, Fu CJ, Li XH. The molecular mechanism of CoenzymeQ10 on pyroptosis and its related diseases: A review. *Protein Pept Lett*. 2022;29(11):911–6.

18. Huang Y, Xu W, Zhou R. NLRP3 inflammasome activation and cell death. *Cell Mol Immunol.* 2021;18(9):2114–27.
19. Li S et al. NLRP3/caspase-1/GSDMD-mediated pyroptosis exerts a crucial role in astrocyte pathological injury in mouse model of depression. *JCI Insight.* 2021;6(23).
20. Taru V, et al. Inflammasomes in chronic liver disease: hepatic injury, fibrosis progression and systemic inflammation. *J Hepatol.* 2024;81(5):895–910.
21. Stoess C, et al. Pyroptosis and gasdermins-Emerging insights and therapeutic opportunities in metabolic dysfunction-associated steatohepatitis. *Front Cell Dev Biol.* 2023;11:1218807.
22. Xian H, et al. Oxidized DNA fragments exit mitochondria via mPTP- and VDAC-dependent channels to activate NLRP3 inflammasome and interferon signaling. *Immunity.* 2022;55(8):1370–e13858.
23. Paradies G, et al. Oxidative stress, Cardiolipin and mitochondrial dysfunction in nonalcoholic fatty liver disease. *World J Gastroenterol.* 2014;20(39):14205–18.
24. Caielli S, et al. Oxidized mitochondrial nucleoids released by neutrophils drive type I interferon production in human lupus. *J Exp Med.* 2016;213(5):697–713.
25. Shang D, et al. mtDNA maintenance and alterations in the pathogenesis of neurodegenerative diseases. *Curr Neuropharmacol.* 2023;21(3):578–98.
26. Sok SPM, et al. 1'-Acetoxychavicol acetate inhibits NLRP3-dependent inflammasome activation via mitochondrial ROS suppression. *Int Immunopharmacol.* 2021;33(7):373–86.
27. Wu QR, et al. IP3R2-mediated Ca(2+) release promotes LPS-induced cardiomyocyte pyroptosis via the activation of NLRP3/Caspase-1/GSDMD pathway. *Cell Death Discov.* 2024;10(1):91.
28. Piamsiri C, et al. Potential roles of IP(3) receptors and calcium in programmed cell death and implications in cardiovascular diseases. *Biomolecules.* 2024;14(10).
29. Alshawish MA, et al. A comparison of the gene expression profiles of non-alcoholic fatty liver disease between animal models of a high-fat diet and methionine-choline-deficient diet. *Molecules.* 2022;27(3).
30. Pi D, et al. Atractylodes lancea rhizome polysaccharide alleviates MCD Diet-Induced NASH by inhibiting the p53/mTOR pathway. *Int J Mol Sci.* 2024;25(20).
31. Shu YY, et al. Rifaximin alleviates MCD diet-induced NASH in mice by restoring the gut microbiota and intestinal barrier. *Life Sci.* 2024;357:123095.
32. Chang W, et al. Isolation and culture of hepatic stellate cells from mouse liver. *Acta Biochim Biophys Sin (Shanghai).* 2014;46(4):291–8.
33. Wu L, Chen J. Type 3 IP3 receptor: its structure, functions, and related disease implications. *Channels (Austin).* 2023;17(1):2267416.
34. Verma A, et al. The role of the mitochondrial protein VDAC1 in inflammatory bowel disease: a potential therapeutic target. *Mol Ther.* 2022;30(2):726–44.
35. Lu Y, et al. Gelsolin's protective role in MASH through F-Actin regulation and P53 degradation. *Adv Sci (Weinh).* 2025;12(23):e2416489.
36. Zhu W, et al. Activation of hepatic adenosine A1 receptor ameliorates MASH via inhibiting SREBPs maturation. *Cell Rep Med.* 2024;5(3):101477.
37. Xu B, et al. Gasdermin D plays a key role as a pyroptosis executor of non-alcoholic steatohepatitis in humans and mice. *J Hepatol.* 2018;68(4):773–82.
38. Ding N, et al. AGK regulates the progression to NASH by affecting mitochondrial complex I function. *Theranostics.* 2022;12(7):3237–50.
39. Wang Y, et al. Hepatocyte Ninjurin2 promotes hepatic stellate cell activation and liver fibrosis through the IGF1R/EGR1/PDGF-BB signaling pathway. *Metabolism.* 2023;140:155380.
40. Picca A, et al. Mitochondrial quality control mechanisms as molecular targets in cardiac ageing. *Nat Rev Cardiol.* 2018;15(9):543–54.
41. Li Q, et al. Oxidized mitochondrial DNA activates the cGAS-STING pathway in the neuronal intrinsic immune system after brain ischemia-reperfusion injury. *Neurotherapeutics.* 2024;21(4):e00368.
42. Eftekhar Z, Aghaei M, Saki N. DNA damage repair in megakaryopoiesis: molecular and clinical aspects. *Expert Rev Hematol.* 2024;17(10):705–12.
43. Xian H, Karin M. Oxidized mitochondrial DNA: a protective signal gone awry. *Trends Immunol.* 2023;44(3):188–200.
44. McArthur K, et al. BAK/BAX macropores facilitate mitochondrial herniation and mtDNA efflux during apoptosis. *Science.* 2018;359(6378).
45. Mangla A, Guerra MT, Nathanson MH. Type 3 inositol 1,4,5-trisphosphate receptor: A calcium channel for all seasons. *Cell Calcium.* 2020;85:102132.
46. Xue Y, et al. SMARCA4/2 loss inhibits chemotherapy-induced apoptosis by restricting IP3R3-mediated Ca(2+) flux to mitochondria. *Nat Commun.* 2021;12(1):5404.
47. Yan H, et al. Hexokinase 2 senses Fructose in tumor-associated macrophages to promote colorectal cancer growth. *Cell Metab.* 2024;36(11):2449–67.e6.
48. Torfi E, et al. Evaluation of Pro-BNP biomarker in heart failure patients and its relationship with complete blood count parameters: A case-control study. *Health Sci Rep.* 2024;7(9):e70083.
49. Ren L, et al. Tryptanthrin suppresses multiple inflammasome activation to regulate NASH progression by targeting ASC protein. *Phytomedicine.* 2024;131:155758.
50. Liu H, et al. Cryptotanshinone specifically suppresses NLRP3 inflammasome activation and protects against inflammasome-mediated diseases. *Pharmacol Res.* 2021;164:105384.
51. Yu J, et al. Zhongfeng Xingnao prescription alleviates injury of intracerebral hemorrhage via regulating the CaMKII/NF-κB p65/NLRP3/GSDMD signaling axis. *J Tradit Complement Med.* 2025;15(1):84–92.
52. Latif MU, et al. NFATc1 signaling drives chronic ER stress responses to promote NAFLD progression. *Gut.* 2022;71(12):2561–73.
53. Friedman SL, et al. Mechanisms of NAFLD development and therapeutic strategies. *Nat Med.* 2018;24(7):908–22.
54. Karimi F, Aghaei M, Saki N. Impact of genetic polymorphisms on treatment outcomes of proteasome inhibitors and immunomodulatory drugs in multiple myeloma. *Curr Treat Options Oncol.* 2025;26(3):197–212.

Publisher's note

Springer Nature remains neutral with regard to jurisdictional claims in published maps and institutional affiliations.